Front. Chem. China 2008, 3(2): 182–185
DOI 10.1007/s11458-008-0035-y

RESEARCH ARTICLE

Xiaolan SONG, Xi HE, Haiping YANG, Dayu XU, Nan JIANG, Guanzhou QIU

Kinetics of thermal decomposition of CeO_2 nanocrystalline precursor prepared by precipitation method

Abstract The thermal decomposition of CeO_2 nanocrystalline precursor prepared by chemical precipitation method was investigated using thermo-gravimetric/differential scanning calorimetry (TG/DSC) and X-ray powder diffraction (XRD). In particular, the differential thermal analysis curves for the decomposition of CeO_2 nanocrystalline precursor were measured at different heating rates in air by a thermal analyzer (NETZSCH STA 449C, Germany). The kinetic parameters of the thermal decomposition of CeO_2 nanocrystalline precursor were calculated using the Kissinger method and the Coats-Redfern method. Results show that the apparent active energy E of the reaction is 105.51 kJ/mol, the frequency factor $\ln A$ is 3.602 and the reaction order n is 2. This thermal decomposition process can be described by the anti-Jander equation and a three-dimensional diffusion mechanism.

Keywords CeO_2 nanocrystals, thermal decomposition kinetics, thermo-gravimetric/differential scanning calorimetry (TG/DSC)

Cerium oxide is a cheap and widely used rare earth material. Due to its superior ability in oxygen conduction and storage, high temperature oxygen vacancy diffuses. CeO_2 can be extensively used in redox reactions and it has become a prospective automobile tail gas purifier catalysis material [1,2], hyperthermia oxygen tolerance material [3,4], pH transducer material [5], solid oxide fuel cell (SOFC) material [6–8], electrochemistry reaction promoting material [9], chemistry machinery polishing (CMP) grinding material [10,11], coating material and doping agent for inoxidizable and corrosion-resistant metal [12], etc. CeO_2 has many potential applications in modern materials science.

The purpose of this study is to define the most probable mechanics function $f(\alpha)$, derive the activation energy E, frequency factor A, calculate the rate constant k and present the expression of reaction rate $d\alpha/dt$ from the TA curves [13]. These parameters serve as the basis for the description of the surface characteristics of the reaction process, determination of the thermal stability of new materials and determination of the reaction mechanism. In this paper, the differential thermal analysis curves were measured at different heating rates in air for the decomposition of the CeO_2 nanocrystalline precursor, and the decomposition process of the CeO_2 nanocrystalline precursor was studied by self-programming software and XRD analysis.

1 Experimental

All reactants were of analytical grade. With cerous nitrate and sal volatile as the raw materials, the mix solution was prepared by adding the sal volatile liquor into the cerous nitrate liquor with a molar ratio of 0.1 mol/L, while 2 g PEG4000 was added into the solution to inhibit hydrolyzation. Then, the mixed solution was stirred at 40°C for 10 minutes with a stirring speed of 800 r/min. The precursor sols were filtered, washed with distilled water and ethanol, dispersed by ultrasonic bath and dried at 343 K to get the pure $Ce_2(CO_3)_3 \cdot H_2O$ powder.

The pyrolytic decomposition of the precursor $Ce_2(CO_3)_3 \cdot H_2O$ was analyzed using a thermal analysis apparatus (NETZSCH STA 499C) produced by NETZSCH Gerätebau GmhH. The TG-DSC curves were obtained in the temperature range 298–823 K at heating rates of 3, 5, 10, 15, 20 K/min. The decomposition kinetics of the CeO_2 nanocrystalline precursor was studied by self-programming software and Matlab.

Tanslated from *Journal of Central South University* (*Science and Technology*), 2007, 38(3): 428–432 [译自: 中南大学学报 (自然科学版]

Xiaolan SONG (✉), Xi HE, Haiping YANG, Dayu XU, Nan JIANG, Guanzhou QIU
Department of Inorganic Materials, School of Resources Processing and Bioengineering, Central South University, Changsha 410083, China
E-mail: xlsong@hnu.cn

2 Results and discussion

2.1 The decomposition process of the CeO_2 nanocrystalline precursor

Figure 1 shows the TG-DSC curves of the CeO_2 nanocrystalline precursor at a heating of 5 K/min. The decomposition process occurs in two steps. Below 373 K, an endothermic peak representing the hydrolysis of the precursor was observed. The theoretical weight loss rate of this process is 3.77%. Between 523 K and 623 K, there is an exothermic peak corresponding to the decomposition of $Ce_2(CO_3)_3$ to CeO_2. The theoretical weight loss rate of this process is 25.22%. So the theoretical weight loss rate of the pyrolytic decomposition is 28.99%. From the TG curves, the experimental weight loss is 29.12% giving a relative error of 0.45%. The pyrolytic decomposition of the precursor was inferred by TG/DSC curves as follows:

First step:

$$Ce_2(CO_3)_3 \cdot H_2O \rightarrow Ce_2(CO_3)_3 + H_2O \quad (1)$$

Second step:

$$Ce_2(CO_3)_3 \rightarrow 2CeO_2 + 2CO_2\uparrow + CO\uparrow \quad (2)$$

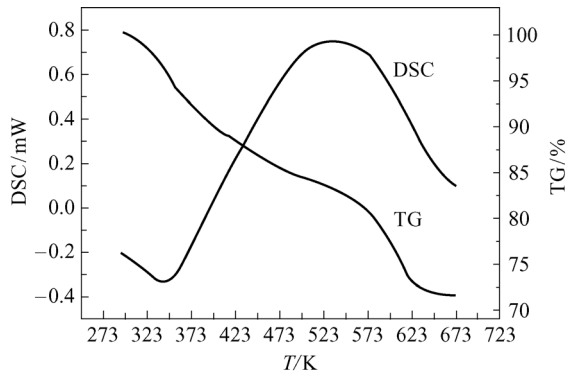

Fig. 1 DSC/TG curves of CeO_2 nanocrystalline precursor at 5 K/min

Figure 2 shows the DSC curves of the CeO_2 nanocrystalline precursor at different heating rates. As shown in Fig. 2, the peaks of DSC curves obtained from different heating rates had the apical temperature hysteresis and the peak area increases as the heating rates increase. Different decomposition rates at different heating rates were observed.

Figure 3 shows the XRD patterns of the precursor powders that calcined at 473 K and 573 K for 1 h. The results of XRD patterns showed that, $Ce_2(CO_3)_3$ was oxidized to $Ce(CO_3)_2$. Minute quantities of CeO_2 were generated when the sample was calcined at 473 K for 1 h but the sample was totally oxidized when the calcination was done at 573 K for 1 h. From the XRD data, it can be concluded that the process of $Ce_2(CO_3)_3 \cdot H_2O$ transformation to CeO_2 involves the oxidation to $Ce_2(CO_3)_2$, then the decomposition to CeO_2. These results are consistent with the TG-DSC analysis.

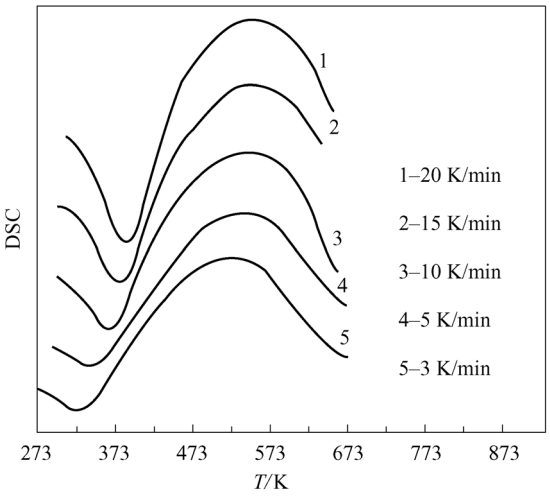

Fig. 2 DSC curves of CeO_2 nanocrystallite precursor at different heating rates

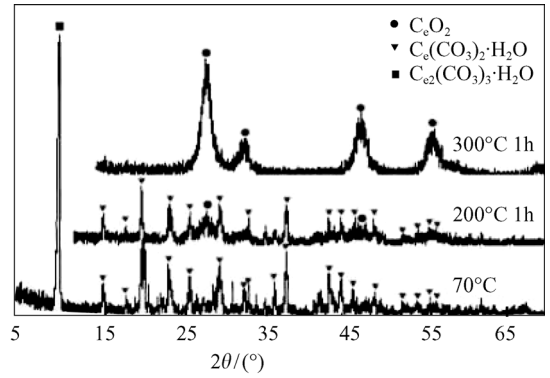

Fig. 3 XRD patterns of precursor at different temperature

TG-DSC and XRD analysis suggest that the pyrolytic decomposition of the precursor is composed of the following steps: hydrolysis of the precursor below 373 K, oxidation to $Ce(CO_3)_2$ after calcination at 473 K, then decomposition to CeO_2 after calcination at 573 K.

2.2 Thermal decomposition kinetics of the CeO_2 nanocrystalline precursor

2.2.1 Differential method

In this paper, the basic non-isothermal kinetic expression was applied to the thermal decomposition kinetics [14],

$$\frac{d\alpha}{dT} = kf(\alpha) \quad (3)$$

$$f(\alpha) = (1-\alpha)^n \quad (4)$$

Equation (3) is the differential equation for dynamics, and equation (4) is the non-isothermal kinetic expression.

Using the Arrhenius equation [15],

$$k = A\exp\left(-\frac{E}{RT}\right) \tag{5}$$

a series of transformations were done on equations (3), (4), (5) to get the equation by Kissinger [14] below,

$$\frac{E\frac{\mathrm{d}T}{\mathrm{d}t}}{RT_p^2} = An\left(1-\alpha_p\right)^{n-1}\exp\left(-\frac{E}{RT_p}\right) \tag{6}$$

where α is the percent conversion of reaction; A, the frequency factor; T, the absolute temperature; β, the heating rate, E, the activation energy, R, the gas constant (8.314 J·mol/K) and n, the reaction order.

If the max reaction rate of the decomposition coincides with the peak of the DSC curves, then α_p and T_p, the percent conversion and temperature, are also at their peak values. From Kissinger's study, $n(1-\alpha_p)^{n-1}$ is independent of β and the value of this expression is equal to 1. Equation (6) becomes

$$\frac{E\beta}{RT_p^2} = A\exp\left(-\frac{E}{RT_p}\right) \tag{7}$$

Logarithmic transformation of equation (7) gives us

$$\ln\left(\frac{\beta_i}{T_{pi}^2}\right) = \ln\frac{AR}{E} - \frac{E}{RT_{pi}},\ (i = 1,2,3,4\ldots) \tag{8}$$

Equation (8) is the Kissinger equation. The peak temperature T_p can be obtained from the DSC curves at different heating rates(Table 1). Linear regression analysis of $\ln(\beta_i/T^2_{pi})$ vs. $1/T_{pi}$ (Fig. 4) was done to obtain the E_k from the slope coefficient and A_k from the intercept. The energy of the endothermic peak E_k is 108.99 kJ/mol and the correlation coefficient is 0.99416.

Table 1 Peak temperature at different heating rates

Heating rate/K·min^{-1}	3	5	10	15	20
Peak temp./K	512.72	520.13	533.21	541.56	550.85

2.2.2 Integration method

The Coats-Redfern [16] integration equation is

$$\ln\frac{G(\alpha)}{T^2} = \ln\frac{AR}{\beta E} - \frac{E}{RT} \tag{9}$$

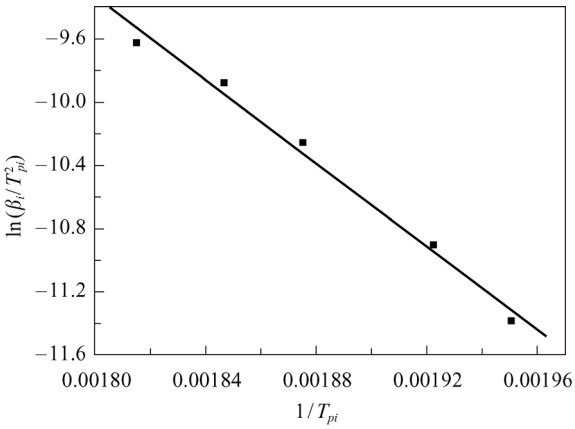

Fig. 4 Fitting lines for Kissinger method

In this equation, α is the percent conversion of the reaction, A, the frequency factor, T, the absolute temperature, β, the heating rate, E, the activation energy, R, the gas constant (8.314 J·mol/K), n, the reaction order and $G(\alpha)$, the integration equation of the decomposition mechanics.

With the self-programming software and Matlab method and using the data in Table 2, regression analysis of $\ln\frac{G(\alpha)}{T^2}$ vs. $\frac{1}{T}$ using the 40 equations from reference [13] was performed. The kinetic parameters E and $\ln A$, the correlation coefficient r, and the standard deviation of the fit Q from these calculations are listed in Table 3.

The mechanism of pyrolytic decomposition was predicted by comparing the result of the Kissinger method and Coats-Redfern method [17]. The equation which gave an E the closest which is 108.99 kJ/mol was taken as the most likely equation for the reaction under study. According to the data above, the 7th equation was coincided with the decomposition process of the precursor. The equation pattern of the decomposition is $G(\alpha) = \left[(1+\alpha)^{\frac{1}{3}} - 1\right]^2$. The process can be described by the anti-Jander equation and is consistent with a three-dimensional diffusion mechanism. The integral and differential form of the anti-Jander equation are $[(1+\alpha)^{1/3} - 1]^2$ and $3/2((1+\alpha)^{2/3}[(1+\alpha)^{1/3} - 1]^{-1}$. Using these equations, values of 102.01 kJ/mol for E, 3.602 for $\ln A$ and 2 for n are obtained.

The calculation was done using the point-by-point method, so the accumulated error is inevitable. The decomposition energy was calculated by averaging the values obtained using the two methods and was found to be 105.50 kJ/mol.

Table 2 Basic data of DSC during thermal decomposition kinetics

No.	1	2	3	4	5	6	7	8	9	10	11	12
T/K	512.4	548.9	563.9	581.4	593.9	608.9	613.9	618.9	623.9	628.9	633.9	638.9
α	0.0524	0.0126	0.2133	0.3032	0.3831	0.4522	0.5100	0.6349	0.7076	0.7937	0.8564	0.9480

Table 3 Parameters of values of thermal decomposition kinetics

No.	E/kJ·mol^{-1}	ln$A$/A·s^{-1}	r	Q
1	129.22	6.950	9.896	0.356
2	27.37	−1.950	9.779	0.003
3	139.05	7.599	9.857	0.573
4	29.75	−1.779	9.720	0.052
5	148.58	8.165	9.813	0.862
6	135.55	6.909	9.873	0.482
7	102.01	3.602	9.926	0.157
8	194.11	1.251	9.541	3.766
9	126.04	−3.326	9.233	0.027
10	20.09	−2.488	9.437	0.050
11	26.08	−1.866	9.510	0.073
12	35.06	−0.974	9.569	0.114
13	50.04	0.452	9.618	0.205
14	57.53	1.148	9.633	0.261
15	79.99	3.199	9.659	0.466
16	124.92	7.209	9.683	1.053
17	169.86	11.158	9.694	1.878
18	259.69	18.975	9.704	4.235
19	349.55	26.736	9.709	7.539
20	−20.33	−5.255	6.629	5.916
21	5.68	−4.318	9.564	0.003
22	10.87	−3.617	9.780	0.005
23	21.23	−2.485	9.868	0.012
24	83.42	5.815	9.926	0.111
25	71.88	1.795	9.760	0.261
26	69.36	1.670	9.788	0.213
27	69.36	2.147	9.788	0.213
28	64.59	1.370	9.836	0.141
29	64.59	1.671	9.836	0.141
30	34.93	−1.093	9.787	0.054
31	23.66	−2.172	9.376	0.078
32	15.96	−2.975	8.693	0.083
33	58.43	1.783	7.572	2.581
34	12.06	7.144	9.139	2.913
35	24.28	−1.773	6.951	0.640
36	−104.15	−12.770	8.907	2.871
37	−198.45	−20.943	8.817	11.44
38	126.71	8.472	7.820	10.359

3 Conclusions

(1) The pyrolytic decomposition of the precursor is composed of two steps: hydrolysis of the precursor below 373 K followed by decomposition to CeO_2 after calcination at 573 K for 1 h.

(2) The kinetic parameters calculated using the Kissinger method and the Coats-Redfern method are: $E = 105.5$ kJ/mol, $\ln A = 3.602$, $n = 2$.

(3) The decomposition of the CeO_2 nanocrystalline precursor follows a three-dimensional diffusion mechanism, and can be described by the anti-Jander equation.

Acknowledgements This work was supported by the International Cooperation Project of Science and Technology Ministry of China (Grant No. 2005DFBA028) and the National Natural Science Foundation of China (Grant No. 59925412).

References

1. Dong X T, Liu G X, Sun J, Hong G Y. Preparation of CeO_2 nanoparticles hydrosol. Rare Metal Materials and Engineering, 2002, 31(3): 229–231
2. Kaspar J, Fornasiero M, Graziani M. Use of CeO_2-based oxides in the three-way catalysis. Catal Today, 2000, 50: 285–298
3. Noriya Izu, Woo suck Shin, Norimitsu Murayama. Resistive oxygen gas sensors based on CeO_2 fine powder prepared using mist pyrolysis. Sensors and Actuators B, 2002, 87: 95–98
4. Zhang M, Wei Z F, Du X Y, Zhang H J, Li W Ch. Effect of CeO_2 coating on oxygen sensitivity of TiO_2 sensor. Chinese Journal of Rare Metals, 2001, 25(1): 71–74
5. Shuk P, Ramanujachary K V. Greenblatt M. New metal-oxide-type pH sensors. Solid State Ionics, 1996, 88: 1115–1120
6. Toshiyuki Mori, John Drennan, Wang Yarong, et al. Influence of nano-structure on electrolytic properties in CeO_2 based system. Journal of Thermal Analysis and Calorimetry, 2002, 70: 309–319
7. Steele B C H. Appraisal of $Ce_{1-y}Gd_yO_{2-y/2}$ electrolytes for IT-SOFC operation at 500°C. Solid State Ionics, 2000, 129: 95–110
8. Murray E P, Tsai T, Barnett S A. A diect methane fuel cell with a ceria based a node. Nature, 1999, 400: 649–651
9. Dong X T. Preparation and application in electrochemistry of the CeO_2 nanocrystalline. Chinese Science Bulletin, 1996, 41(9): 847–850
10. Joseph M S, Shyam P M, Ronald J G. Chemical mechanical planarization of microelectronic materials. New York: John Wiley & Sons Inc, 1997. 41
11. Hoshino T, Kurata Y, Terasaki Y, Susa K. Mechanism of polishing of SiO_2 films by CeO_2 particles. Journal of Non-Crystalline Solids, 2001, 283: 129–136
12. Ma Y H. Current status and prospects of rare earth applications in china. Materials Review, 2000, 14(1): 3–5
13. Hu R Z, Shi Q Z. Thermal Analysis Kinetic. Beijing: Science Press, 2001
14. Sestak J, Berggren G. Study of the kinetics of the mechanism of solid-state reactions at increasing temperatures. Thermochimica. Acta, 1971, 3(1): 1–12
15. Kissinger H E. Reaction kinetics in differential thermal analysis. Analalytical Chemistry, 1957, 29(11): 1702–1706
16. Coats A W, Redfern J P. Kinetic parameters from thermogravimetric data. Nature, 1964, 201:68–69
17. Muraishi K, Suzuki Y, Kiruchi A. Kinetics of the thermal decomposition of dicarboxylic acids. Thermochimica Acta, 1994 (239): 51–59